Oxygen diffusion in ellipsoidal tumor spheroids

David Robert Grimes[1,2], Frederick J. Currell [1],

1 Centre for Advanced and Interdisciplinary Radiation Research (CAIRR) School of Mathematics and Physics, Queen's University Belfast, BT7 1NN, Northern Ireland, UK.

2 Cancer Research UK/MRC Oxford Institute for Radiation Oncology, Gray Laboratory, University of Oxford, Old Road Campus Research Building, Of Roosevelt Drive, Oxford, OX3 7DQ, UK.

* d.r.grimes@qub.ac.uk

Abstract

Oxygen plays a central role in cellular metabolism, in both healthy and tumor tissue. The presence and concentration of molecular oxygen in tumors has a substantial effect on both radiotherapy response and tumor evolution, and as a result the oxygen micro-environment is an area of intense research interest. Multicellular tumor spheroids closely mimic real avascular tumors, and in particular they exhibit physiologically relevant heterogeneous oxygen distribution. This property has made them a vital part of in vitro experimentation. For ideal spheroids, their heterogeneous oxygen distributions can be predicted from theory, allowing determination of cellular oxygen consumption rate (OCR) and anoxic extent. However, experimental tumor spheroids often depart markedly from perfect sphericity. There has been little consideration of this reality. To date, the question of how far an ellipsoid can diverge from perfect sphericity before spherical assumptions breakdown remains unanswered. In this work we derive equations governing oxygen distribution (and more generally, nutrient and drug distribution) in both prolate and oblate tumor ellipsoids, and quantify the theoretical limits of the assumption that the spheroid is a perfect sphere. Results of this analysis yield new methods for quantifying OCR in ellipsoidal spheroids, and how this can be applied to markedly increase experimental throughput and quality.

Author summary

Multicellular tumor spheroids (MCTS) are an increasingly important tool in cancer research, exhibiting non-homogeneous oxygen distributions and central necrosis. These are more similar to *in situ* avascular tumors than conventional 2D biology, rendering them exceptionally useful experimental models. Analysis of spheroids can yield vital information about cellular oxygen consumption rates, and the heterogeneous oxygen contribution. However, such analysis pivots on the assumption of perfect sphericity, when in reality spheroids often depart from such an ideal. In this work, we construct a theoretical oxygen diffusion model for ellipsoidal tumor spheroids in both prolate and oblate geometries. With these models established, we quantify the limits of the spherical assumption, and illustrate the effect of this assumption breaking down. Methods of circumventing this are also presented, and the analysis here suggests new methods for expanding experimental throughput to also include ellipsoidal data.

Introduction

Oxygen plays a seminal role in cancer treatment and patient prognosis. The presence of molecular oxygen in a tumor markedly increases radio-sensitivity, with well-oxygenated regions responding to radiotherapy up to a factor of three relative to anoxic sub-volumes [1, 2]. This oxygen enhancement ratio is also seen in emerging modalities such as proton therapy [3, 4], raising the tantalizing prospect of dose-painting, where dose is selectively boosted to hypoxic regions to boost therapy response [5]. The basic idea underpinning dose-painting has been discussed for over a decade, but application has been hampered by difficulty in non-invasive hypoxia imaging. Methods such as F-MISO PET have a maximum resolution in the millimetre regime, while oxygenation varies over a micron scale. As a consequence, mathematical modeling is vital for bridging the resolution gap [6].

Aside from therapeutic considerations, oxygen has a marked impact on patient prognosis. The pioneering work of Gray and colleagues in the early 1950s established that tumor oxygen concentration was correlated with prognosis, and extensive hypoxia was a negative prognostic marker [7]. This finding has been well replicated to present day [8–10] and is not solely due to hypoxia-induced treatment resistance. Under severe hypoxia, tumor cells can respond to such pressure by activating oxygen-sensitive signaling pathways [11, 12]. Current biological thinking suggests these signalling pathways act to alter gene expression to promote cell survival under adverse conditions. Hypoxia is also a major driver of angiogenesis, giving rise to new routes for cells to travel along [13, 14], endowed with the ability to metastasize [15].

The extraordinary importance of oxygen in cancer treatment and evolution has made it an important avenue of study, with an urgent need for further research. Despite the fundamental importance of molecular oxygen in tumors, investigations have been complicated by the significant experimental difficulty in ascertaining oxygen concentration *in situ* [6]. Real tumors have highly heterogeneous oxygen supply and complex tortured vasculature, and even well-oxygenated regions are frequently inter-spaced with pockets of anoxia [14, 16]. Standard 2D monolayers of cells are not an ideal experimental model, typically exhibiting an unrealistically homogeneous oxygen contribution. There is however a more realistic experimental option in the form of tumor spheroids. These clusters of cancer cells grow in approximately spherical 3D aggregates, and exhibit signalling and metabolic profiles more similar to real tumors than is observed in monolayer approaches [17–19].

Like monolayers, spheroids are relatively easy to culture, and growing interest has seen them used for a variety of purposes, including radiobiological application as a means to test fractionation [20–23], as a model for drug delivery [24–28], for investigation of the stem-cell hypothesis [29] and for exploring FDG-PET dynamics [30] for hypoxia in solid tumors. Crucially, the non homogeneous oxygen distributions in tumor spheroids have been well studied [31–33]. Research to date shows cellular oxygen consumption rate (OCR) has a known influence on the oxygen concentration throughout a spheroid, and directly influences the extent of central anoxia, and the viable rim thickness by known mathematical relationships [32], and thus measuring these aspects allows an experimenter to determine OCR with relative ease compared to other methods [28].

Such methods and the underlying theory are exceptionally important to understanding the factors that influence tumor oxygen distribution, yet all these methods rely on an implicit assumption of perfect sphericity. There is a clear rationale behind this, as symmetry considerations simplify the problem greatly. Yet in experimental conditions,

imperfect spheroids are common, frequently growing as extended ellipsoids. When the eccentricity of these shapes is extreme, an experimenter may reasonably choose to discard them from analysis. But this prompts a question; quite how extreme do such deformations have to be before a spherical assumption breaks down? Presumably small departures from sphericity should not impact analysis, where as highly eccentric ellipsoids could reasonably be presumed to violate the underlying theoretical assumptions. The question of how such eccentricities might skew analysis of spheroids, and how trustworthy results of such analyis might be has not yet been considered in literature, despite its obvious practical importance.

These questions are as of yet unanswered, and are of paramount importance given the growing adoption of spheroids for cancer research, and their utility in estimating OCR [31, 32]. Knowing the acceptable limits of eccentricity for spheroid analysis would be of considerable benefit to experimenters, providing error estimates and limits of reliability. A full analytic expression for "ellipsoidals" (analogous to the spherical case) would also be of substantial benefit, allowing the analysis of eccentric shapes and potentially increasing experimental throughput. In this work, we seek to address these issues by deriving an expression for oxygen diffusion in both prolate and oblate geometries. This is contrasted to the spherical case to determine the limits of validity for experimental data, and the implications of this are discussed. A schematic of this is depicted in fig 1.

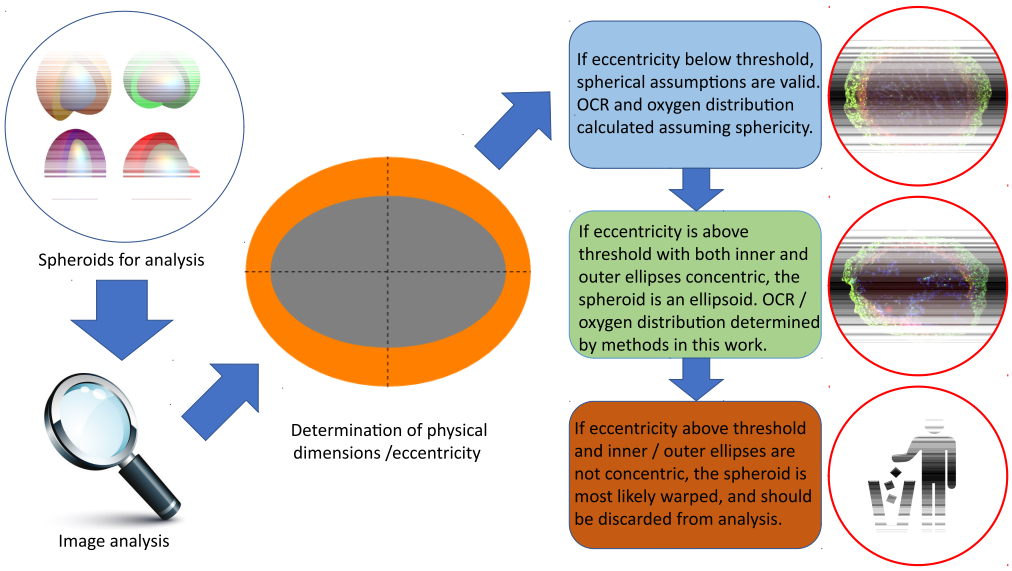

Fig 1. Schematic analysis in this work. Below a calculated threshold for eccentricity, spheroids can be treated as having perfect sphericity without introducing unacceptable error, and their OCR and oxygen distribution established by previously published methods [32]. At greater eccentricities however, a spherical assumption is no longer valid. If the inner and outer sections are concentric ellipses, these can be analyzed by the methods outlined in this work to ascertain OCR and oxygen distribution. If eccentricity is higher than a threshold value, and inner and outer ellipses are not concentric, this suggests the spheroid is severely warped or the section if off the central axis, and should be discarded from analysis. See text for details.

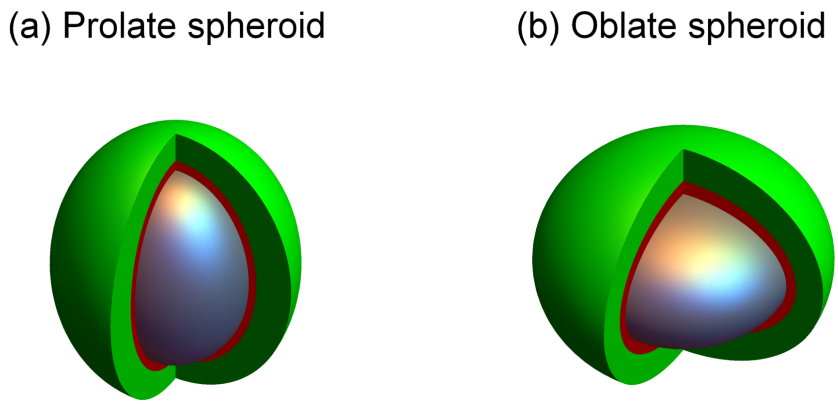

Fig 2. (a) Prolate spheroid (b) Oblate spheroid. The anoxic central core in both cases ($e = 0.75$) is depicted in gray, and the hypoxic extent in red, whilst well oxygenated cells are shown in green. Both ellipsoids have the same volume necrotic core, but their resultant oxygen distributions are slightly different. See text for discussion.

Spheroids and Ellipsoids

The general equation of an ellipsoid is given by

$$\frac{x^2}{a^2} + \frac{y^2}{b^2} + \frac{z^2}{c^2} = 1 \tag{1}$$

where a, b and c are the major axes' lengths. For an ellipsoid with azimuthal symmetry, $a = b$. Where all axis are equal ($a = b = c$), the result is a perfect sphere. To date, this is the only case which has been well-studied from a theoretical standpoint [31–33]. Whilst the mathematical treatments to date have assumed spheroids are perfect spheres, the nomenclature 'spheroid' still applies to the more general case, including prolate and oblate spheroids. In this work we broaden the mathematical framework to be applicable to ellipsoids without full spherical symmetry, which are namely

1. Prolate spheroids: In the case where $c > a$, the resulting ellipsoid is an ellipse rotated around its major axis, the line joining its foci. This yields a rugby ball type shape.

2. Oblate spheroids: where $a > c$, an oblate spheroid results, equivalent to an ellipse rotated around its minor axes. The resulting shape is discus-like.

Examples of these ellipsoids are shown in fig 2.

Model derivation

Prolate spheroids

In a prolate spherical geometry, the prolate spherical coordinate system is most natural to employ. We shall use a geometrically intuitive definition where curves of constant σ are prolate spheroids, whilst curves of constant τ correspond to hyperboloids of revolution [34]. The full derivation is presented in supplementary material **S1**, and the full solution for oxygen partial pressure in terms of σ is

$$P_{Prolate}(\sigma) = \frac{a\Omega f^2}{6D}\left(\sigma^2 - \sigma_n^2 + \log\left(\frac{\sigma^2-1}{\sigma_n^2-1}\right) + \sigma_n^3 \log\left(\frac{(1+\sigma)(1-\sigma_n)}{(1-\sigma)(1+\sigma_n)}\right)\right) \tag{2}$$

where σ_n corresponds to the innermost ellipsoidal surface with $p(\sigma_n) = 0$, $a\Omega$ is oxygen consumption rate in mmHg/s, f is distance from ellipse centre to foci and $D = 2 \times 10^{-9}$ m^2/s, the oxygen diffusion constant in water. Alternatively, an equivalent solution can be be defined with respect to the outer-most ellipsoidal surface, σ_o where $P(\sigma_o) = p_o$. The solution can then be written as

$$P_{Prolate}(\sigma) = p_o + \frac{a\Omega f^2}{6D}\left(\sigma^2 - \sigma_o^2 + \log\left(\frac{\sigma^2-1}{\sigma_o^2-1}\right) + \sigma_n^3 \log\left(\frac{(1+\sigma)(1-\sigma_o)}{(1-\sigma)(1+\sigma_o)}\right)\right). \tag{3}$$

Equations 2 and 3 are equivalent, and the choice of which to employ depends on whether the problem is specified by the inner or outermost ellipse.

Oblate spheroids

In oblate spherical geometry, a similar geometrical definition exists [35] and can be solved through similar methods, also outlined in supplementary material **S1**. The full solution in terms of σ for an oblate spheroid is

$$\begin{aligned} P_{Oblate}(\sigma) = \frac{a\Omega f^2}{6D}\Bigg(&\sigma^2 - \sigma_n^2 + 4\log\left(\frac{\sigma}{\sigma_n}\right) + \\ &2(\sigma_n^2+2)(\sqrt{\sigma_n^2-1})\left(\arctan\left(\frac{1}{\sqrt{\sigma^2-1}}\right) - \arctan\left(\frac{1}{\sqrt{\sigma_n^2-1}}\right)\right)\Bigg). \end{aligned} \tag{4}$$

Similarly, this can be defined instead in terms of the outer ellipsoidal surface by

$$\begin{aligned} P_{Oblate}(\sigma) = p_o + \frac{a\Omega f^2}{6D}\Bigg(&\sigma^2 - \sigma_o^2 + 4\log\left(\frac{\sigma}{\sigma_o}\right) + \\ &2(\sigma_n^2+2)(\sqrt{\sigma_n^2-1})\left(\arctan\left(\frac{1}{\sqrt{\sigma^2-1}}\right) - \arctan\left(\frac{1}{\sqrt{\sigma_o^2-1}}\right)\right)\Bigg). \end{aligned} \tag{5}$$

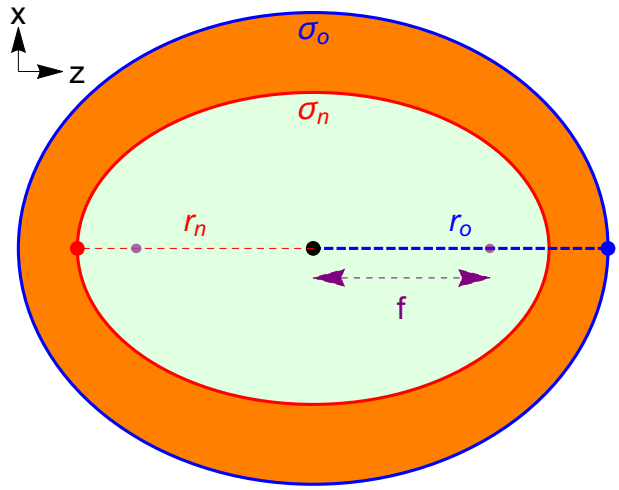

Fig 3. Geometry of an ellipsoid and relation to Cartesian coordinates

Translation to Cartesian coordinates and concentricity

The above equations define the partial pressure on confocal ellipsoidal surfaces, but it is usually more intuitive to work in Cartesian coordinates. Ellipsoid geometry is illustrated in fig 3. In both prolate and oblate spherical coordinates, the point (z, x) converts to σ, given by

$$\sigma = \frac{1}{2f}\left(\sqrt{x^2 + (z+f)^2} + \sqrt{x^2 + (z-f)^2}\right). \tag{6}$$

By definition, a constant σ denotes an ellipsoidal surface. It can also be shown σ is the inverse of the ellipse's eccentricity e, a proof of which is given in supplementary material **S1**. If the outer ellipsoid and inner ellipsoid at the anoxic boundary have eccentricities of e_o and e_n respectively, then

$$\sigma_o = 1/e_o. \tag{7}$$
$$\sigma_n = 1/e_n.. \tag{8}$$

Analogous to the perfect spherical case, concentric elliptical surfaces of constant σ are at the same oxygen partial pressure. For any concentric ellipsoid,

$$e_c r_c = f. \tag{9}$$

will hold, where e_c is the ellipsoid eccentricity and r_c the semi-major axis length.It follows the innermost (anoxic) and outermost ellipsoids should also be concentric, so within the bounds of acceptable experimental error, $e_o r_o \approx e_n r_n$. This relationship can be used to determine whether a given spheroid displaying apparent eccentricity is an ellipsoid or not. This is important from an experimental perspective, as sectioning can introduce serious distortions in fixed spheroid sections, or can miss the central axis of the spheroid [32]. In these cases, an ostensible ellipsoid might be observed, but may in fact be a sectioning distortion or off-centre cut. Testing for concentricity can thus determine the underlying reality. This point is elaborated upon in the discussion section.

Methods

Ellipsoid oxygen profiles

The models derived in this work were used to create oxygen profiles for ellipsoids of both prolate and oblate classes, which were contrasted to conventional spherical profiles.

Quantifying differences between prolate and oblate cases

Prolate and oblate forms have some mathematical differences as can be seen inspection of equations 2 - 5 inclusive. If all else is kept constant, prolate and oblate spheroids will have a slightly different value for σ_n, and thus different volumes for their anoxic core. Whether this difference is significant experimentally is an important question; from a single projection of a tumor ellipsoid it might be impossible to ascertain whether an experimenter is dealing with a prolate or oblate case. As an experimentalist might not be able to determine whether a given ellipsoid is prolate or oblate from a single section, quantifying differences in measured OCR under each assumption is an important goal of this work. This effect was simulated by producing prolate and oblate ellipsoids with properties as outlined in table 1, producing two different estimates of anoxic inner ellipsoidal shell denoted σ_{np} and σ_{no}, corresponding to the values determined for the prolate and oblate case, equations 3 and 5 respectively. OCR estimates under the 'wrong' assumption (applying either oblate equations for a prolate spheroid or vice versa) were then calculated by solving $P_{Prolate}(\sigma_{no}) = 0$ and $P_{Oblate}(\sigma_{np}) = 0$ respectively. These 'wrong' OCR estimates were then compared to known OCR to assess the error introduced by an incorrect assumption.

Comparisons with spherical case

As OCR from spheroids is estimated assuming spherical symmetry, a major aspect of this work was quantifying precisely how close to perfect sphericity spheroids must be so that such an assumption holds, and how departures from sphericity impact estimates of OCR and oxygen profiles. To study this, ellipsoids with known OCR and varying eccentricity were simulated. As the distance from the ellipsoid centre to the outer ellipsoidal shell at any angle of θ is related to the semi-major axis by $r_o\sqrt{1 - e^2 \sin^2 \theta}$, then the average centroid to ellipsoidal shell distance can be calculated by the mean value of the function over the interval $[0, 2\pi]$, and simplifies to

$$\langle r_o \rangle = \frac{2 r_o E_m(e^2)}{\pi} \tag{10}$$

where $\langle r_o \rangle$ is the average distance of the centroid to the outer ellipsoidal shell, and E_m is the complete elliptic integral of the second kind. A similar method yields $\langle r_n \rangle$, the average distance of centroid to the inner anoxic boundary. The standard deviations (Δr_o and Δr_n respectively) for the function were calculated by a similar method to yield

$$\Delta r_o = \sqrt{\frac{1}{2\pi} \int_0^{2\pi} (r_o \sqrt{1 - e^2 \sin^2 \theta} - \langle r_o \rangle)^2 d\theta} = \sqrt{r_o^2 \left(1 - \frac{e^2}{2}\right) - \langle r_o \rangle^2}. \tag{11}$$

In a perfectly spherical case, OCR (in mmHg/s) is related to the anxoic radius r_n and outer radius r_o by

$$a\Omega = \frac{6Dp_o}{r_o^2 + \frac{2r_n^3}{r_o} - 3r_n^2}. \tag{12}$$

For perfect spheroids, this is easily calculated. For ellipsoids with small eccentricity this should provide a good approximation of true OCR. However an outstanding question is how far from sphericity can a spheroid depart before this approximation is no longer adequate. To determine this, ellipsoids (both prolate and oblate) of varying semi-major axis and known OCR were simulated. These were then analysed using the spherical approximation, where Δr_o and Δr_n were treated as experimental error. By standard error propagation techniques, the projected error in the OCR estimate under this assumption is given by

$$\Delta a\Omega = \frac{12Dp_o\sqrt{(\langle r_o\rangle^2 + \langle r_o\rangle\langle r_n\rangle + \langle r_n\rangle^2)^2(\Delta r_o)^2 + 9\langle r_o\rangle^2\langle r_n\rangle^2(\Delta r_n)^2}}{(\langle r_o\rangle - \langle r_n\rangle)^3(\langle r_o\rangle + 2\langle r_n\rangle)^2}. \tag{13}$$

The spherical OCR and perpetuated error was contrasted with the true known ellipsoidal OCR to determine the limits of such an approximation in different cases, and to estimate at what point spherical approximations are no longer appropriate.

OCR estimation in ellipsoids

For any tumor ellipsoid, it is possible to estimate OCR from physical extent analogous to the spherical case in equation 12. For the prolate case, this is

$$a\Omega = \frac{6Dp_o}{r_o^2 - r_n^2 + e_o^2 r_o^2 \log\left(\frac{e_n^2(1-e_o^2)}{e_o^2(1-e_n^2)}\right) + \frac{r_n^2}{e_n}\log\left(\frac{(e_o+1)(e_n-1)}{(e_o-1)(e_n+1)}\right)}. \tag{14}$$

For oblate spheroids, OCR is given by

$$a\Omega = 6Dp_o\Bigg(r_o^2 - r_n^2 + 4e_o^2 r_o^2 \log\left(\frac{r_n}{r_o}\right) + 2r_n^2(1+2e_n^2)\sqrt{\frac{1-e_n^2}{e_n^2}}\left(\arctan\left(\frac{e_o}{\sqrt{1-e_o^2}}\right) - \arctan\left(\frac{e_n}{\sqrt{1-e_n^2}}\right)\right)\Bigg)^{-1}. \tag{15}$$

An example of the implementation of this is included in the code included in supplementary material **S2**.

Results

Oxygen distributions in ellipsoids

Ellipsoidal tumors were simulated with properties shown in table 1. Unlike for the spherical case, the oxygen profile in ellipsoids is not radially symmetric. Examples of these profiles are depicted in fig 4. Oxygen gradients through ellipsoids are simulated in fig 5, for both prolate and oblate cases with increasing eccentricity, where the z axis is aligned with the semi-major axis and the x-axis with semi-minor.

Table 1. Simulation parameters

Parameter	Simulation value
Semi-major axis	500 μm
Oxygen consumption rate (a)	20 mmHg/s
External partial pressure (p_o)	100 mmHg

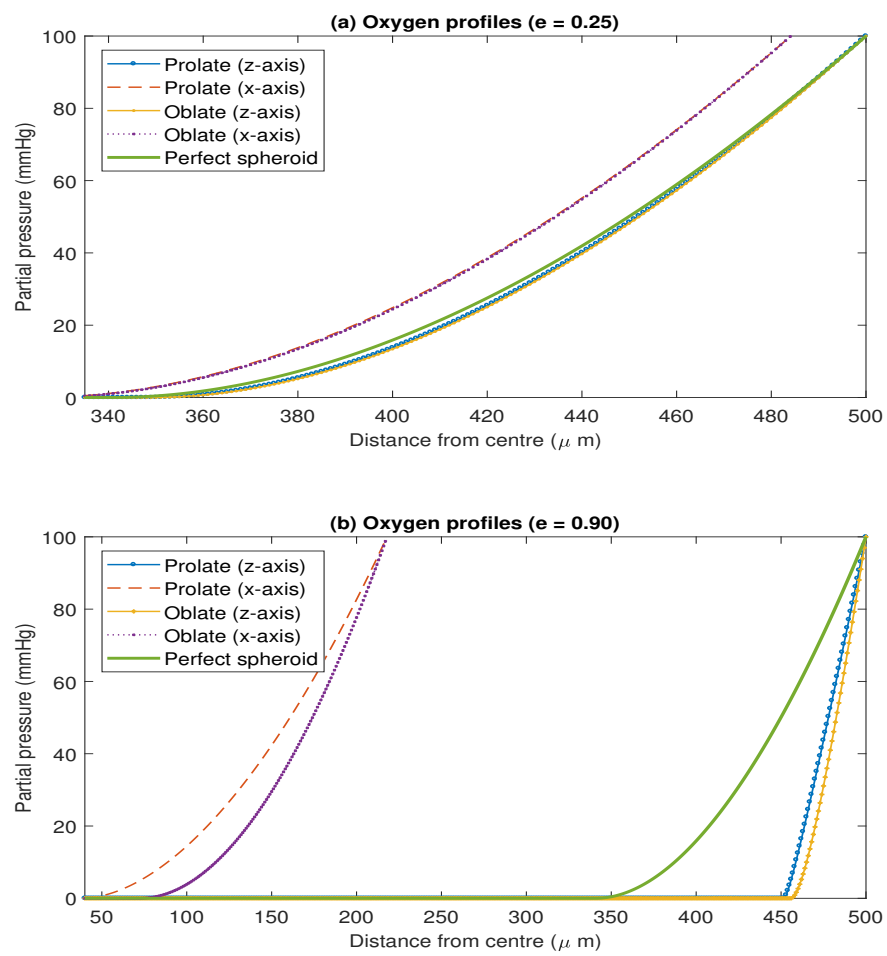

Fig 4. (a) Oxygen profiles for both prolate and oblate ellipsoids with e = 0.25 along the z and x axis.(b) Oxygen profiles for both prolate and oblate ellipsoids with e = 0.90 along the z and x axis. Perfect spherical case is symmetric in z and x by definition.

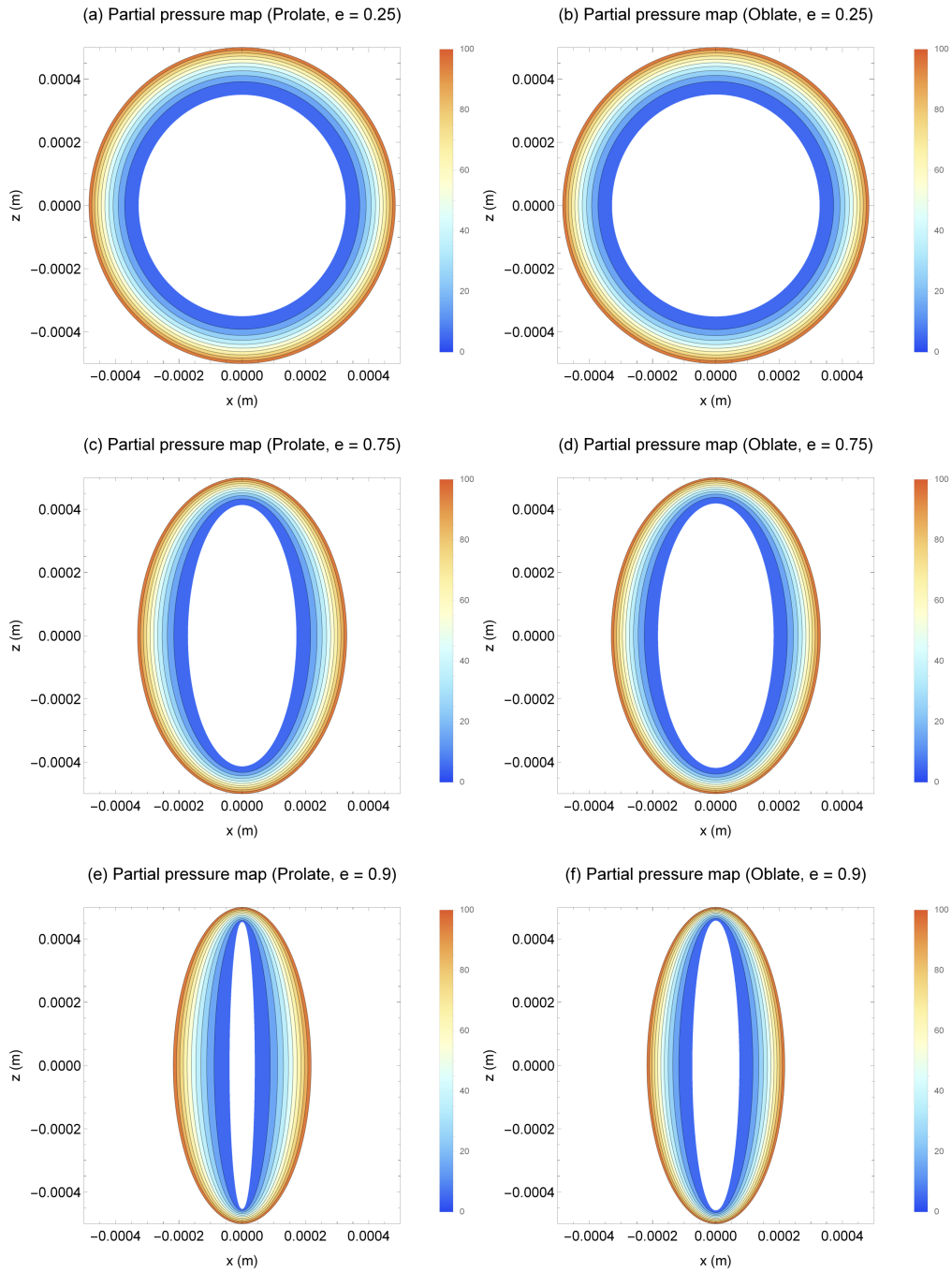

Fig 5. (a) - (f) - Contour oxygen maps for prolate and oblate ellipsoids with increasing eccentricity with semi-major axis 500μm and OCR of 20 mmHg/s. Prolate and oblate have broadly similar oxygen maps, with divergence manifesting as $e \to 1$

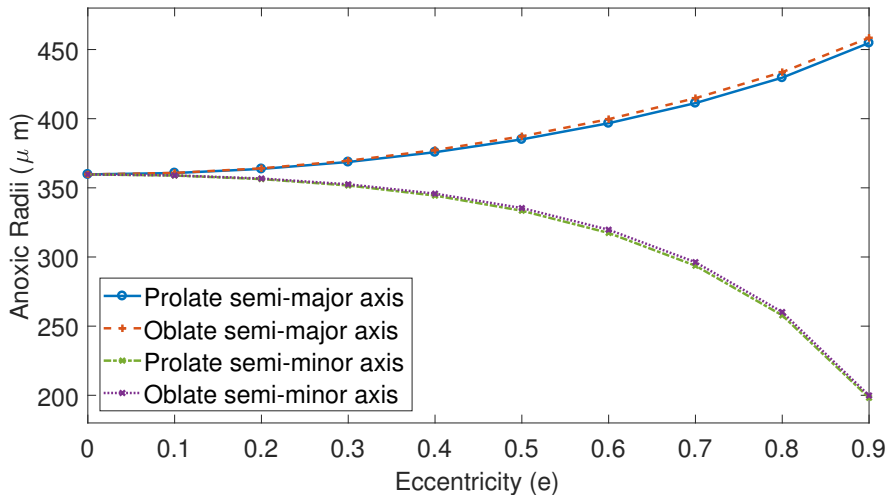

Fig 6. Variation of anoxic radii with eccentricity for spheroid with properties as per table 2.

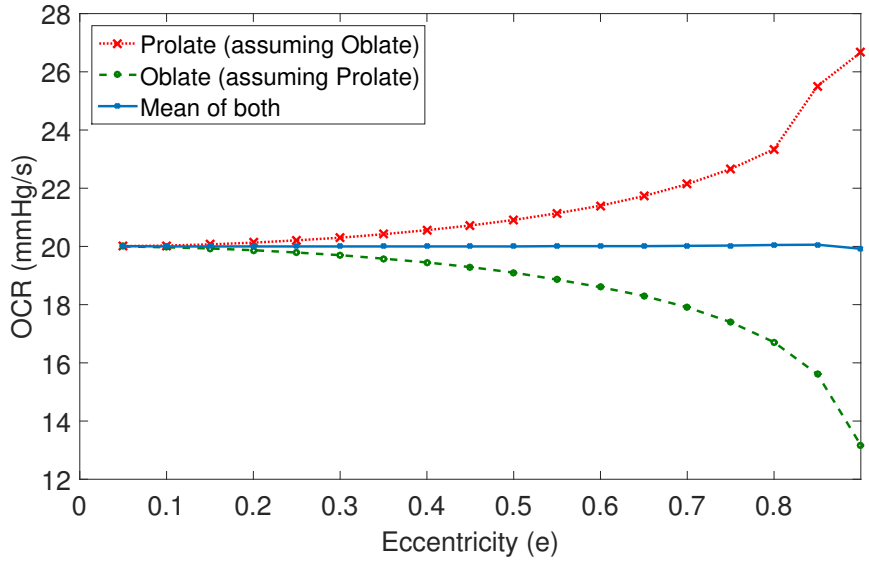

Fig 7. OCR estimates under 'wrong' assumptions. True OCR is 20 mmHg/s.

Quantification of differences in prolate and oblate ellipsoids

From 2D sectioning or imagining alone, it can be experimentally difficult to ascertain whether a given ellipsoid is either prolate or oblate. It is thus important to quantify differences between the ellipsoids. figs 4 and 5 suggest that prolate and oblate ellipsoids have broadly similar oxygen profiles until eccentricity approaches unity. fig 6 depicts internal anoxic radii with eccentricity. These differ only slightly, typically $\leq 1\%$ for both major and minor axis for $0 < e < 0.9$. More interesting perhaps is the variation in OCR estimate with eccentricity under the 'wrong' assumption (namely assuming oblate form when actual entity is prolate or vice versa) shown in fig 7. This suggests strongly that OCR estimates arrived at under the 'wrong' assumption are still accurate up until high

eccentricity. Even at very high eccentricity, an average value of both incorrect OCRs was extremely close to true OCR. This suggests that incorrectly specifying the type of ellipsoid should not greatly impact OCR estimates.

Comparison of spheroids and ellipsoids (OCR estimation)

fig 8 depicts the impact of assuming perfect sphericity on OCR estimates for properties in table 1. At low e, treating ellipsoids as spheroids yields acceptable accuracy for OCR estimates (defined here as an OCR estimate encapsulating true OCR with $\frac{\Delta a\Omega}{a\Omega} \leq 0.1$ and ≤ 0.25). However, as $e \to 1$, the reliability of OCR estimates employing equation 13 rapidly break-down, as seen in table 2 for various different true OCRs and major-axis lengths.

Table 2. Acceptable eccentricity threshold for assuming perfect sphericity

Semi-major axis (μm)	OCR (mmHg/s)	e ($\frac{\Delta a\Omega}{a\Omega} \leq 0.10$)	e ($\frac{\Delta a\Omega}{a\Omega} \leq 0.25$)
500	10	0.27	0.41
	15	0.25	0.38
	20	0.23	0.36
	25	0.22	0.34
	30	0.21	0.33
1000	10	0.19	0.30
	15	0.18	0.28
	20	0.16	0.26
	25	0.15	0.24
	30	0.15	0.23

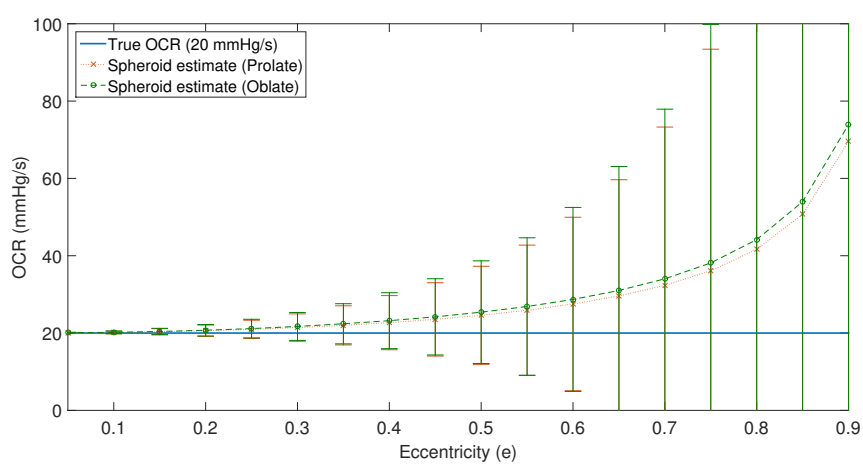

Fig 8. 'Spherical' OCR estimates with increasing eccentricity. At low e, treating an ellipsoid as a perfect spheroid yields acceptable accuracy. However, as $e \to 1$, estimates become increasingly unreliable. Note that the y-axis has been truncated for clarity.

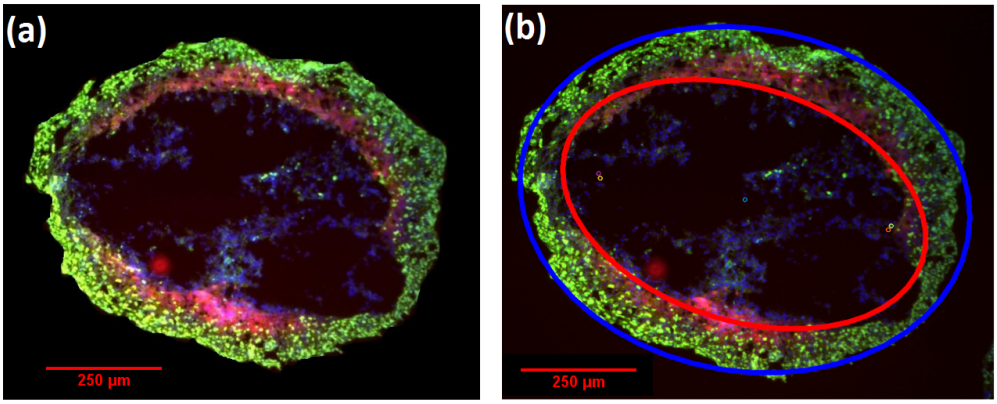

Fig 9. Demonstration of analysis in a DLD-1 tumor ellipsoid. A sample image analysis algorithm detects best-fit ellipses, checking these for concentricity and estimating OCR. See text for details.

Discussion

Analysis of spheroids to date tends to pivot on the presumption of sphericity, as symmetry arguments reduce the complexity required. However, real spheroids tend to depart from perfect sphericity to varying extents. In this work, we provide a metric for determining how reliable the simpler spherical assumption will be as eccentricity increases, as outlined in table 2. In general for smaller spheroids ($r_o \leq 500\mu$m), a threshold value for outer eccentricity of about $e = 0.3$ should keep uncertainty below 25%. For greater accuracy, eccentricity must be below this (table 2. Because of these limits, the methods outlined in this work can be employed to generate reliable estimates of OCR and oxygen distribution. Another major benefit of this work is that it allows an experimenter to determine OCR even in non-spherical cases when high eccentricity might otherwise render the spheroids in question ill-suited for analysis. Provided the inner and outer ellipses are approximately concentric, the analysis outlined in this work can be employed, and thus should help increase experimental throughput.

To date, non-spherical tumor ellipsoids have been somewhat neglected, frequently discarded from analysis due to their inherent uncertainty. It is thus difficult to find ellipsoidal tumor spheroid data. A potential example is shown in fig 9, from a previously analyzed set of sectioned DLD-1 tumor spheroids [32]. These were dual-stained with proliferation marker Ki-67 (in green) and EF5 (a hypoxia marker which binds between $0.8 \leq p \leq 10$ mmHg, shown by the red staining), and were experimentally determined to have an OCR of 22.10 ± 4.24 mmHg/s. The illustrated spheroid was excluded from analysis because of its high eccentricity ($e_o \approx 0.66$, $r_o = 488.5\mu$m), however, as the best-fit inner and outer ellipses are concentric ($e_o r_o \approx e_n r_n$) we can assume this is a valid spheroid and apply methods outlined in this work to analyze it as a proof of concept. Table 3 shows estimated OCR for this ellipsoid under different assumptions.

As depicted in the table, attempting a spherical analysis yields completely unrealistic results for OCR and massive uncertainty, as predicted in this work. When analysed as either prolate or oblate spheroids however, OCR estimates are in agreement with the previously measured values. This is promising, but as only a single data point is available, this should be interpreted solely as a proof of concept

Table 3. OCR estimates for sample spheroid

Assumption	Estimated OCR (mmHg/s)
Previously measured for DLD-1 cell-line	22.10 ± 4.24
Assumption of perfect sphericity (true spheroid)	67.17 ± 117.19
Assuming prolate tumor spheroid	26.76 ± 7.13
Assuming oblate tumor spheroid	24.01 ± 6.40

It's worth noting that from single section images or microscopy, there is no obvious way to ascertain whether a ellipsoid is prolate or oblate. As the mathematical forms for these are slightly different, this adds an extra uncertainty and prompts the question about which form is preferable to employ. The analysis in this work (figs 6 and 7) indicate that even if one incorrectly assumes the wrong form, OCR estimates are still very good, with only minimal errors introduced. This holds with only negligible errors until very high eccentricity. It is also possible to average different, which tends to produce a more reliable result when the underlying form is unknown, as demonstrated in fig 7.

There are a number of potential confounding influences and caveats that need to be considered before the methods in this work can be employed. While modeling of elliptical oxygen diffusion has the potential to greatly extend experimental throughput, there are a number of scenarios where an ostensible ellipsoid might not be what it appears. For fixed and sectioned spheroids, the act of sectioning itself can be enough to induce substantial deformations, stretching it along a particular axis. Ostensibly, the resultant shape might appear an ellipsoid, but is in fact a warped spheroid, and thus cannot be reliably analyzed with the methods outlined. From the mathematics established in this work, we can distinguish between true ellipsoids and warped spheroids - if the inner and outer ellipses are not concentric ($e_o r_o \approx e_n r_n$), then the shape is likely a warped spheroid. Results under either spherical or ellipsoidal assumptions are likely to be misleading, and these should be discounted from analysis, as per fig 1. The concentric condition derived in this work provides a rapid way to ascertaining whether a spheroid is externally warped, and whether to discount it.

There is a more subtle issue with sectioned spheroids, which becomes even more crucial with sectioned ellipsoids. Analysis for both spheroids and ellipsoids relies on a section through the central axis of the spheroid. In the spherical case, if the section is off centre, the net result will be two concentric circles but with a misleading ratio, rendering any OCR calculation derived from this suspect. By contrast, any plane through an ellipsoid produces an ellipse, but if these cuts are off the central axis, then the inner and outer ellipses will not longer have a common centre, and will not be concentric. In this regard, determining an off-centre ellipsoid section is relatively straight-forward. A proof of this is provided in supplementary **S1**.

The theoretical analysis outlined here presents biological investigators with new methods for extending spheroid analysis, and means to interpret data which departs from sphericity. It also establishes uncertainty bounds for on existing spherical analysis techniques, and methods for determining OCR and oxygen distribution in tumor ellipsoids. The findings of this work will increase experimental confidence with tumor spheroids, and has the potential to substantially increase experimental throughput, improving our insights on everything from tumor hypoxia to drug delivery. Such an approach is imperative if we are to fully exploit this unique experimental tool, and ultimately marshal the new insights obtained towards better cancer treatment and

diagnostics.

Supporting information

S1 Appendix. Mathematical appendix and full derivations.

S2 Appendix. Sample code for ellipsoid oxygen distribution and OCR calculation (Mathematica, MATLAB / Octave)

Acknowledgments

References

1. Grimes DR, Partridge M. A mechanistic investigation of the oxygen fixation hypothesis and oxygen enhancement ratio. Biomedical Physics and Engineering Express. 2015;1(4):45209. doi:10.1088/2057-1976/1/4/045209.
2. Hall EJ, Giaccia AJ, et al. Radiobiology for the Radiologist. vol. 6. Lippincott Williams & Wilkins Philadelphia:; 2006.
3. Wenzl T, Wilkens JJ. Modelling of the oxygen enhancement ratio for ion beam radiation therapy. Physics in Medicine & Biology. 2011;56(11):3251.
4. Grimes DR, Warren DR, Partridge M. An approximate analytical solution of the Bethe equation for charged particles in the radiotherapeutic energy range. Scientific reports. 2017;7(1):9781.
5. Bentzen SM, Gregoire V. Molecular imaging–based dose painting: A novel paradigm for radiation therapy prescription. In: Seminars in radiation oncology. vol. 21. Elsevier; 2011. p. 101–110.
6. Grimes DR, Warren DR, Warren S. Hypoxia imaging and radiotherapy: bridging the resolution gap. The British Journal of Radiology. 2017;(December 2016):20160939. doi:10.1259/bjr.20160939.
7. Gray LH, Conger A, Ebert M, Hornsey S, Scott O. The concentration of oxygen dissolved in tissues at the time of irradiation as a factor in radiotherapy. The British journal of radiology. 1953;26(312):638–648.
8. Vaupel P, Thews O, Hoeckel M. Treatment resistance of solid tumors. Medical oncology. 2001;18(4):243–259.
9. Vaupel P, Briest S, Höckel M. Hypoxia in breast cancer: pathogenesis, characterization and biological/therapeutic implications. Wiener Medizinische Wochenschrift. 2002;152(13-14):334–342.
10. Vaupel P, Mayer A, Höckel M. Tumor hypoxia and malignant progression. In: Methods in enzymology. vol. 381. Elsevier; 2004. p. 335–354.

11. Lu X, Kang Y. Hypoxia and hypoxia-inducible factors: master regulators of metastasis. Clinical cancer research. 2010;16(24):5928–5935.

12. Mujcic H, Hill R, Koritzinsky M, Wouters B. Hypoxia signaling and the metastatic phenotype. Current molecular medicine. 2014;14(5):565–579.

13. Sullivan R, Graham CH. Hypoxia-driven selection of the metastatic phenotype. Cancer and Metastasis Reviews. 2007;26(2):319–331.

14. Grimes DR, Kannan P, Warren DR, Markelc B, Bates R, Muschel R, et al. Estimating oxygen distribution from vasculature in three-dimensional tumour tissue. Journal of The Royal Society Interface. 2016;13(116):20160070.

15. Rankin EB, Nam JM, Giaccia AJ. Hypoxia: signaling the metastatic cascade. Trends in cancer. 2016;2(6):295–304.

16. Secomb TW, Hsu R, Park EY, Dewhirst MW. Green's function methods for analysis of oxygen delivery to tissue by microvascular networks. Annals of biomedical engineering. 2004;32(11):1519–1529.

17. Hirschhaeuser F, Menne H, Dittfeld C, West J, Mueller-Klieser W, Kunz-Schughart LA. Multicellular tumor spheroids: an underestimated tool is catching up again. Journal of biotechnology. 2010;148(1):3–15.

18. Gomes A, Guillaume L, Grimes DR, Fehrenbach J, Lobjois V, Ducommun B. Oxygen partial pressure is a rate-limiting parameter for cell proliferation in 3d spheroids grown in physioxic culture condition. PloS one. 2016;11(8):e0161239.

19. Leek R, Grimes DR, Harris AL, McIntyre A. Methods: using three-dimensional culture (spheroids) as an in vitro model of tumour hypoxia. In: Tumor Microenvironment. Springer; 2016. p. 167–196.

20. Santini M, Rainaldi G, Indovina P. Multicellular tumour spheroids in radiation biology. International journal of radiation biology. 1999;75(7):787–799.

21. Dubessy C, Merlin JL, Marchal C, Guillemin F. Spheroids in radiobiology and photodynamic therapy. Critical reviews in oncology/hematology. 2000;36(2):179–192.

22. Madsen SJ, Sun CH, Tromberg BJ, Cristini V, De Magalhães N, Hirschberg H. Multicell tumor spheroids in photodynamic therapy. Lasers in surgery and medicine. 2006;38(5):555–564.

23. Kempf H, Bleicher M, Meyer-Hermann M. Spatio-temporal cell dynamics in tumour spheroid irradiation. The European Physical Journal D. 2010;60(1):177–193.

24. Dufau I, Frongia C, Sicard F, Dedieu L, Cordelier P, Ausseil F, et al. Multicellular tumor spheroid model to evaluate spatio-temporal dynamics effect of chemotherapeutics: application to the gemcitabine/CHK1 inhibitor combination in pancreatic cancer. BMC cancer. 2012;12(1):15.

25. Mehta G, Hsiao AY, Ingram M, Luker GD, Takayama S. Opportunities and challenges for use of tumor spheroids as models to test drug delivery and efficacy. Journal of Controlled Release. 2012;164(2):192–204.

26. Kim TH, Mount CW, Gombotz WR, Pun SH. The delivery of doxorubicin to 3-D multicellular spheroids and tumors in a murine xenograft model using tumor-penetrating triblock polymeric micelles. Biomaterials. 2010;31(28):7386–7397.

27. Vinci M, Gowan S, Boxall F, Patterson L, Zimmermann M, Lomas C, et al. Advances in establishment and analysis of three-dimensional tumor spheroid-based functional assays for target validation and drug evaluation. BMC biology. 2012;10(1):29.

28. Grimes DR, Kannan P, McIntyre A, Kavanagh A, Siddiky A, Wigfield S, et al. The role of oxygen in avascular tumor growth. PloS one. 2016;11(4):e0153692.

29. Fang D, Kim Y, Lee C, Aggarwal S, McKinnon K, Mesmer D, et al. Expansion of CD133+ colon cancer cultures retaining stem cell properties to enable cancer stem cell target discovery. British journal of cancer. 2010;102(8):1265.

30. Kelly CJ, Hussien K, Muschel RJ. 3D tumour spheroids as a model to assess the suitability of [18F] FDG-PET as an early indicator of response to PI3K inhibition. Nuclear medicine and biology. 2012;39(7):986–992.

31. Mueller-Klieser W. Method for the determination of oxygen consumption rates and diffusion coefficients in multicellular spheroids. Biophysical journal. 1984;46(3):343–348.

32. Grimes DR, Kelly C, Bloch K, Partridge M. A method for estimating the oxygen consumption rate in multicellular tumour spheroids. Journal of the Royal Society, Interface / the Royal Society. 2014;11(92):20131124. doi:10.1098/rsif.2013.1124.

33. Grimes DR, Fletcher AG, Partridge M. Oxygen consumption dynamics in steady-state tumour models. Royal Society open science. 2014;1(1):140080.

34. Prolate spheroidal coordinates (Wikipedia entry); 2018. Available from: https://en.wikipedia.org/wiki/Prolate_spheroidal_coordinates.

35. Oblate spheroidal coordinates (Wikipedia entry); 2018. Available from: https://en.wikipedia.org/wiki/Oblate_spheroidal_coordinates.